SCIENTIFIC REPORTS

OPEN

SUBJECT AREAS:
MATERIALS CHEMISTRY
MATERIALS SCIENCE

Received
13 November 2013

Accepted
19 March 2014

Published
3 April 2014

Correspondence and requests for materials should be addressed to X.C.Z. (xzeng1@unl.edu) or Y.F.L. (ylu2@unl.edu)

# Control of crystallographic orientation in diamond synthesis through laser resonant vibrational excitation of precursor molecules

Zhi Qiang Xie[1], Jaeil Bai[2], Yun Shen Zhou[1], Yi Gao[2,3], Jongbok Park[1], Thomas Guillemet[1], Lan Jiang[4], Xiao Cheng Zeng[2] & Yong Feng Lu[1]

[1]Department of Electrical Engineering, University of Nebraska-Lincoln, Lincoln, Nebraska 68588-0511, USA, [2]Department of Chemistry, University of Nebraska-Lincoln, Lincoln, Nebraska 68588-0304, USA, [3]Shanghai Institute of Applied Physics, Chinese Academy of Science, Shanghai 201800, China, [4]School of Mechanical Engineering, Beijing Institute of Technology, Beijing 100081, China.

**Crystallographic orientations determine the optical, electrical, mechanical, and thermal properties of crystals. Control of crystallographic orientations has been studied by changing the growth parameters, including temperature, pressure, proportion of precursors, and surface conditions. However, molecular dynamic mechanisms underlying these controls remain largely unknown. Here we achieved control of crystallographic orientations in diamond growth through a joint experimental and theoretical study of laser resonant vibrational excitation of precursor molecules (ethylene). Resonant vibrational excitation of the ethylene molecules using a wavelength-tunable $CO_2$ laser steers the chemical reactions and promotes proportion of intermediate oxide species, which results in preferential growth of {100}-oriented diamond films and diamond single crystals in open air. Quantum molecular dynamic simulations and calculations of chemisorption energies of radicals detected from our mass-spectroscopy experiment provide an in-depth understanding of molecular reaction mechanisms in the steering of chemical reactions and control of crystallographic orientations. This finding opens up a new avenue for controlled chemical vapor deposition of crystals through resonant vibrational excitations to steer surface chemistry.**

Laser control of chemical reactions through resonant excitations has been extensively studied in bimolecular collisions, unimolecular decompositions, and gas-solid reactions[1–5]. However, the effects of laser control of reactions are usually too weak to be significant for material synthesis[6]. Control of chemical reactions via resonant vibrational excitation of precursor molecules is promising in that molecular vibrations are directly related to the rearrangement of their bonds to become products[1,5]. Lasers are ideal energy sources for vibrational excitations because their narrow bandwidth prepares a single vibrational eigenstate[5], which makes precise control of reaction pathways feasible. One approach to laser control is active intervention, in which the phases of reagent motions are controlled during the course of the reaction[6]. This active intervention may preferentially lead reagents to one of many different reaction routes. In this study, we introduced active intervention to material synthesis, and achieved control of chemical reaction and hence controlled crystallographic orientations through laser resonant vibrational excitations of precursor molecules in chemical vapor deposition (CVD) of diamond.

Due to its extreme properties, diamond has found widespread applications, including heat spreaders, optical windows, biosensors, and nano- or microelectromechanical systems (N/MEMS)[7–10], as well as its promising potentials in quantum information technology[11–13]. Many properties of diamond, including thermal conductivity, optical behavior, and mechanical properties, depend on diamond crystallographic orientations[14,15]. Preferential growth of {100}-textured diamond films has been pursued for years because of their superior properties over those of the {111}- and {110}-textured diamonds[16–23]. Mechanically, {100}-textured diamond films have lower roughness and higher wear resistance as compared with other crystallographic directions[16]. Optical properties of {100}-textured films are superior to those of {111}-textured films in terms of refractive index and extinction coefficient[16]. Research efforts have been exerted to achieve orientation-controlled growth of diamond. Liu *et al.* have studied control of diamond textures by varying the growth parameters, including substrate temperature, precursor

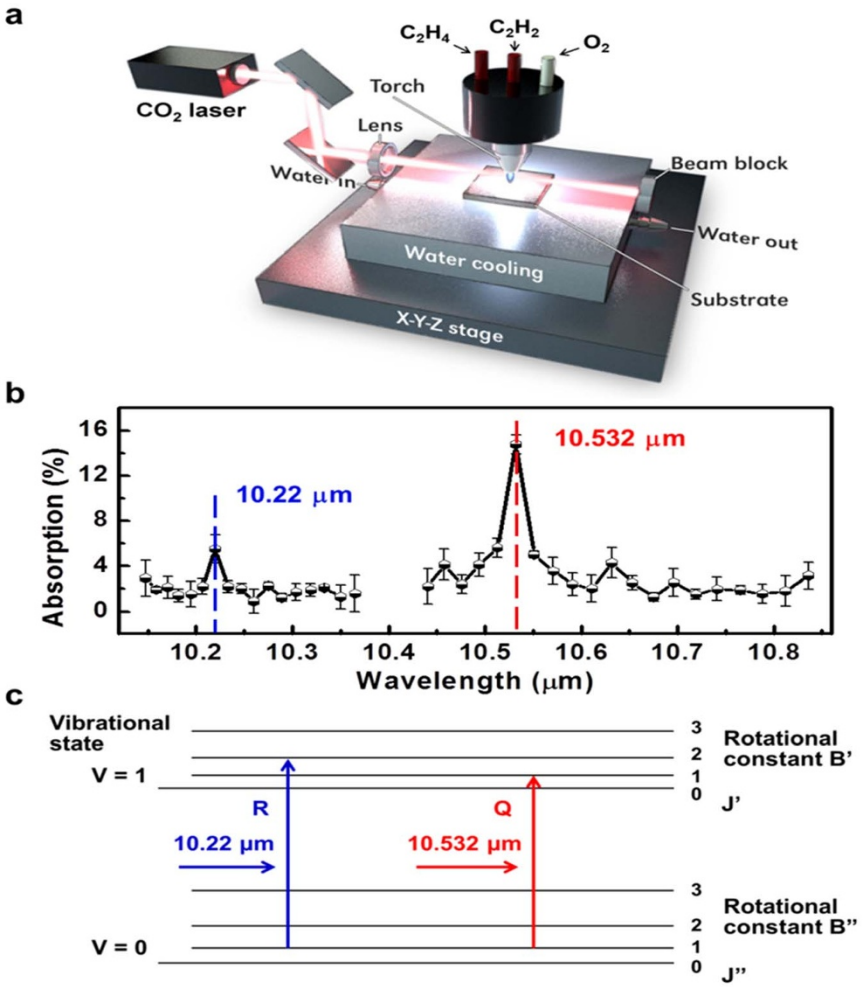


**Figure 1 | Absorption of laser energy by the $C_2H_4/C_2H_2/O_2$ flame.** (a), Schematic of the experimental setup. (b), Absorption of laser energy by the $C_2H_4/C_2H_2/O_2$ flame as a function of laser wavelength in the $CO_2$ laser $00^\circ1–10^\circ0$ emission band. The error bars indicate standard deviations. (c), Vibration-rotation transitions of an ethylene molecule with $CO_2$ laser excitations at different wavelengths, indicating that the $CO_2$ laser at both 10.22 and 10.532 μm excites the molecules to a higher vibrational level, whereas the 10.22 μm excitation provides additional rotational energy in the molecules.

concentration, and films thickness[14]. By applying bias-enhanced nucleation[20,21] and introducing nitrogen into the growth precursors[22–26], {100}-textured diamond films have also been successfully deposited. These methods are capable of producing {100}-textured diamond films with good reproducibility. However, the molecular reaction mechanism remains elusive and further investigations are needed to obtain in-depth understanding on the control of crystallographic orientation. In our previous study, resonant excitations of precursor molecules have been applied in the synthesis of diamond films and crystals[27,28]. Diamond growth rate and quality were obviously promoted. Diamond crystals with sizes up to 5 mm were successfully obtained in open air[28]. In-depth understanding of the laser control of chemical reactions and control of diamond crystallographic orientations are investigated in this research.

## Results and discussion

We introduced resonant excitations of precursor molecules using a wavelength-tunable $CO_2$ laser to steer the chemical reactions in diamond formation which in turn resulted in preferential growth of {100}-textured diamond of high phase purity. The diamond growth process was steered by resonantly exciting ethylene ($C_2H_4$) molecules to higher vibrational and rotational states. A schematic illustration of the experimental setup is shown in Figure 1a. The detailed experimental method is described in the Methods section. The wavelength of the tunable $CO_2$ laser ranges from 9.2 to 10.9 μm. Figure 1b shows a representative absorption spectrum of the laser energy by the $C_2H_4/C_2H_2/O_2$ flame with respect to the laser wavelength in the $CO_2$ laser $00^\circ1–10^\circ0$ emission band. Several absorption peaks were observed at different wavelengths. The strongest peak at 10.532 μm corresponds to the Q branch ($\Delta J = 0$) of a fundamental vibration mode ($\nu_7$, $CH_2$-wagging) of the ethylene molecules[25]. Another absorption peak at 10.22 μm corresponds to the R branch ($\Delta J = 1$) of the $CH_2$-wagging mode[29,30], which means that the molecules are excited to a higher level of vibrational state with a higher level of rotation energy, as schematically indicated in Figure 1c.

We compared the excitations of ethylene molecules in the combustion flame by laser irradiation at 10.22, 10.333 (non-resonant wavelength), and 10.532 μm, and deposited diamond films with all other parameters the same. Figure 2a–d show representative scanning electron microscopic (SEM) images of diamond films deposited for 15 (upper) and 60 min. (lower), respectively. Diamond films deposited without laser excitation were also included for comparison. Thicknesses of these diamond films are given in Figure S1 of the Supporting Information. It was observed that diamond films deposited by the 10.22 μm laser excitation exhibit predominantly {100} surfaces, while those deposited under the other three conditions showed random orientations. This phenomenon does not change with deposition time, as demonstrated by similar film morphology under each condition of different deposition time (15 and 60 min.). It is demonstrated that excitation of ethylene molecules through the

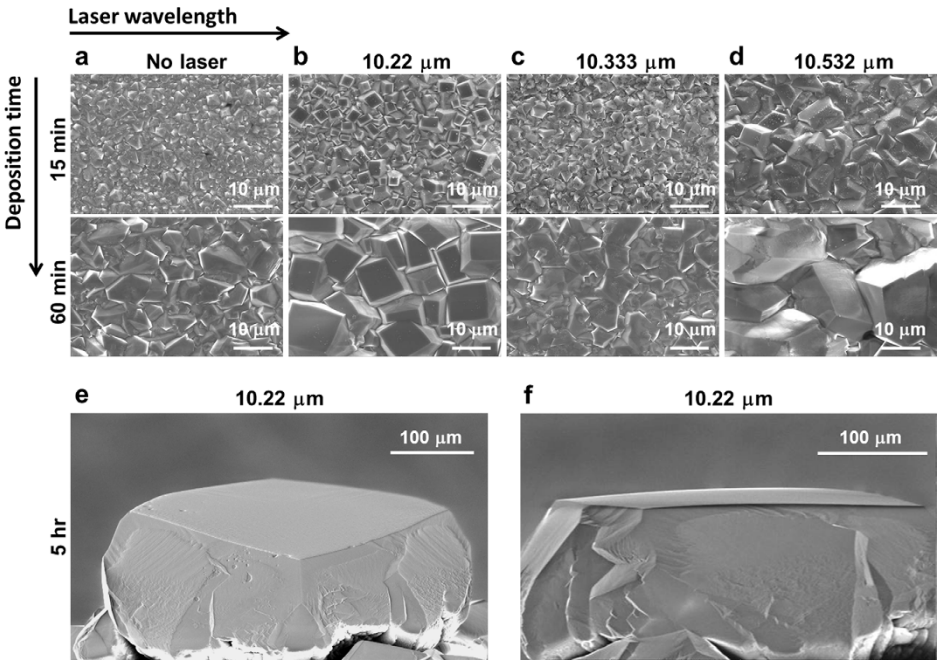


**Figure 2 | SEM images of the diamond morphologies.** (a–d), Diamond films deposited without laser (a), with $CO_2$ laser irradiation at 10.22 (b), 10.333 (c), and 10.532 μm (d). (upper: 15-min. deposition, lower: 60-min. deposition). (e), (f), Single-crystal diamond grown for 5 hr. with $CO_2$ laser excitation at 10.22 μm.

vibrational excitation of ethylene molecules at 10.22 μm leads to a preferential growth of {100}-textured diamond films.

Under the resonant excitation at 10.22 μm, single crystal diamond with a size of 300 μm was grown in 5 hr. in open air, as shown in Figure 2e. Different from the diamond crystals deposited through vibrational excitation of ethylene at 10.532 μm[28], this diamond crystal exhibits high uniformity. A flat {100} surface as shown in Figure 2f demonstrated the preferential growth of the {100} surface for long time deposition. No twinning was observable in the SEM images on the {100} surface. Twinnings abundantly exist on the {111} surfaces (the four surfaces surrounding the {100} surface), which is believed to be caused by the faster growth in the ⟨111⟩ compared to that in the ⟨100⟩ direction[15]. The crystal shape of diamond facets is determined by the growth rate of the ⟨100⟩ direction ($V_{100}$) and that of the ⟨111⟩ direction ($V_{111}$), as indicated by the diamond growth parameter, $\alpha = \sqrt{3}\frac{V_{100}}{V_{111}}$ [14,32]. The facets that show up at the final stage of crystal growth are those along which the growth velocity is the least. The growth velocity of the ⟨111⟩ direction should be greater than that of the ⟨100⟩ direction in order to obtain the predominantly {100} surfaces. It has been widely accepted in diamond growth that higher growth velocity in certain sector will result in lower phase purity in that sector, which results in the twinnings on the {111} surfaces[15,31,32]. A lower concentration of twinnings on the {100} surface indicates high quality of the {100}-oriented diamond crystals.

Raman spectroscopy was performed to determine the phase purity of the deposited diamond films and crystals. Figure 3a shows Raman spectra of the diamond films deposited for 60 min. under different excitation conditions. The shift of the diamond peak from 1332 (phase-pure natural diamond) to 1335 $cm^{-1}$ is ascribed to the residual stresses in the diamond films caused by differences in the coefficients of thermal expansion (CTE) between the diamond films and the substrates. The D-band is related to disordered carbon structures, and G-band corresponds to $sp^2$ graphite phases in the diamond films. It is obvious that both D- and G-bands are suppressed in diamond films deposited with laser excitations at 10.22 and 10.532 μm, indicating an increased purity of diamond $sp^3$ bonding. The spectrum of the diamond film deposited with laser excitations at 10.22 μm exhibits even lower D- and G- bands, indicating that the {100} surfaces have better phase purity than other surfaces. This is in agreement with the transmission electron microscopic (TEM) study of different diamond growth sectors, which revealed that the ⟨100⟩ sector has low density of dislocations, while the ⟨111⟩ sectors are highly defective, containing a high density of dislocations and stacking faults[15]. Figure 3b shows the Raman spectra of diamond crystals, including those deposited with 10.22 (shown in Figure 2e) and 10.532 μm excitations (reported in Ref. 25) as well as a type Ia natural diamond. The diamond peaks of these three crystals are all located at 1332 $cm^{-1}$. The D- and G-bands are invisible in all spectra, which indicate very high purity of the diamond $sp^3$ bonding. The full width at half maximum (FWHM) value of the {100}-oriented diamond is 3.3 $cm^{-1}$, which is similar to that of the natural diamond (3.1 $cm^{-1}$), much narrower than that of the diamond crystal deposited with the 10.532 μm excitation (4.5 $cm^{-1}$). Therefore, the {100}-oriented diamond crystal deposited with vibrational excitation of ethylene at 10.22 μm has high phase purity and high crystal quality.

Mass spectroscopy (MS) of the $C_2H_4/C_2H_2/O_2$ combustion flame used for diamond growth was performed under different excitation conditions to investigate mechanisms of the preferential growth of {100}-textured diamond, with more details described in the Methods section. Ionization of species occurs in the combustion flame, making the flame suitable for direct analysis using MS. Figure 4a shows a representative mass spectrum of the $C_2H_4/C_2H_2/O_2$ flame, in which positive ions with m/z values ranging from 12 to 47 are detected and assigned as $CH_x^+$ ($x = 0 \sim 3$), $C_2H_x^+$ ($x = 0 \sim 5$), $C_3H_x^+$ ($x = 0 \sim 5$), $CH_xO^+$($x = 1 \sim 3$) and $C_2H_xO^+$($x = 2 \sim 5$) ions. Considering differences in ionization potentials among different species, the height of each line does not necessarily represent the absolute concentration of each species. Nevertheless, MS analysis of the flame is valuable to determine the evolvement of species concentration under different excitation conditions, given that the variation of ions is proportional to that of related species. Figure 4b shows a chromatogram of the total ion current (TIC) of the $C_2H_4/C_2H_2/O_2$ flame under different excitation conditions, which provides the intensity of all detected ions in the flame. The TIC of the flame is a summation of all detected ions in the flame. By using the analysis tools as described

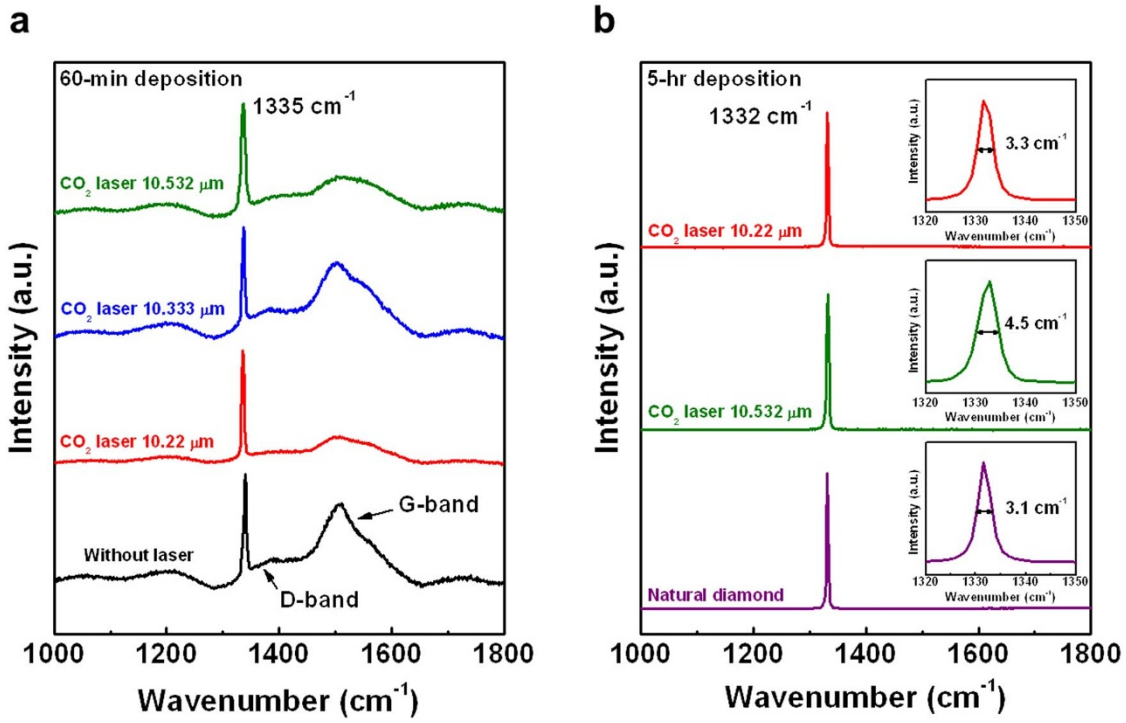


**Figure 3 | Raman spectra of the diamond samples.** (a), Diamond films deposited for 60 min without laser, with $CO_2$ laser excitation at 10.22, 10.333 and 10.532 μm. (b), Diamond crystals grown for 5 hr with $CO_2$ laser excitation at 10.22 and 10.532 μm. Natural diamond (type Ia) is also characterized as comparison. Insets respectively show the FWHM of the diamond peak for each crystal.

in the Methods section, the chromatogram of each detected ion can be derived from the TIC signal. The chromatogram of each ion has similar shape with that of the TIC. Figure S3, given in the Supplementary Information, provides chromatograms of $CH_3^+$, $CH_3O^+$, $C_2H_3^+$, and $C_2H_3O^+$ as examples. The chromatograms of other species (CH, $CH_2$, $C_2H$, $C_2H_2$, $CH_2O$, $C_2H_2O$, etc.) have similar shapes. The intensity of each ion can be obtained by calculating the average value of the corresponding scans. The concentration of each ion was derived by dividing its intensity with the TIC value in order to eliminate the variation of its absolute value in different measurements. Because species containing one or two carbons are of interest to diamond growth[32], relative concentrations of $CH_x^+$ ($x = 0 \sim 3$), $C_2H_x^+$ ($x = 0 \sim 5$), $CH_xO^+$ ($x = 1 \sim 3$), and $C_2H_xO^+$ ($x = 2 \sim 5$) ions were calculated and summarized respectively, as shown in Figures 4c and 4d. The relatively large deviation of the species concentration is mainly caused by flame fluctuation during the mass spectrometry (MS) measurement. The uncertainty caused by the deviation is suppressed in two aspects. Firstly, mass flow controller (MFC) with more precise control was used, which suppressed the flame fluctuation. Secondly, number of the measurements (more than twenty) was increased for each wavelength. The mean value for each wavelength is hence believed to be representative for the trends, although relatively large deviation exists.

In Figure 4c, the concentrations of both $CH_x$ and $C_2H_x$ species were increased by laser excitations at 10.22 and 10.532 μm. The $CH_xO$, and $C_2H_xO$ species show similar trends, as shown in Figure 4d. However, a detailed comparison between Figure 4c and 4d reveals a slight difference between the species intensities with laser excitations at 10.22 and 10.532 μm. Concentrations of the $CH_x$ and $C_2H_x$ species are the highest at 10.532 μm, whereas those of the $CH_xO$ and $C_2H_xO$ species are the highest at 10.22 μm. As discussed in the beginning of this section, the excitation of ethylene molecules by the $CO_2$ laser at 10.22 μm corresponds to the R branch ($\Delta J = 1$) of the $CH_2$-wagging mode, which means that the molecules are excited to a higher level of vibrational state with a higher level of rotation energy. Because the energy transfer by the rotational-translational channel through binary molecular collision is much faster than that by the rotational-vibrational channel[33], higher rotational energy will result in higher translational energy, which is reflected by higher temperature. That means the excitation of ethylene molecules by the $CO_2$ laser at 10.22 μm resulted in higher flame temperature than the excitations at other wavelengths (with same quantity of laser energy absorbed). The increased flame temperature consequently resulted in promoted oxidation of the carbon hydride species. In other words, concentration of the oxygen-containing species ($CH_xO$, $C_2H_xO$, etc.) was increased by higher flame temperature caused by the 10.22 μm $CO_2$ laser excitation. This explanation has been confirmed by quantum molecular dynamics (QMD) simulations for exploration of intermediate species in the $C_2H_4/C_2H_2/O_2$ flames, shown in Movie S1 and summarized in Figure S4. It is indicated in the simulation that as the temperature of the flame is increased, the $CH_xO$ ($x = 1 \sim 3$) and $C_2H_xO$ ($x = 2 \sim 5$) species appear with larger population through the combustion process. Details of the QMD simulation are given in the Supplementary Information.

To gain molecular insights into relative abundances of produced species on different diamond surface, we computed the chemisorption energies of all species detected in the mass spectrometry experiment ($CH_x$ ($x = 0 \sim 3$), $C_2H_x$ ($x = 0 \sim 5$), $CH_xO$ ($x = 1 \sim 3$), and $C_2H_xO$ ($x = 2 \sim 5$)) on the diamond C{100} and C{111} surface, respectively. Periodic density-functional theory (DFT) methods are employed (see Methods section). The chemisorption energies are shown in Table 1. Note that the chemisorption capacity can be used as an indicator of surface reactivity[34,35]. Stronger chemisorptions lead to higher surface reaction activity. As shown from Table 1, the chemisorption of all species (except $C_2H_5O$ with the least population, which is due to the perfect bond-length match with the C{100}-$2 \times 1$ reconstruction surface) on the C{111} surface is much stronger than on the C{100} surface, indicating higher reactivity on C{111} surface and hence higher growth in the ⟨111⟩ direction than that in

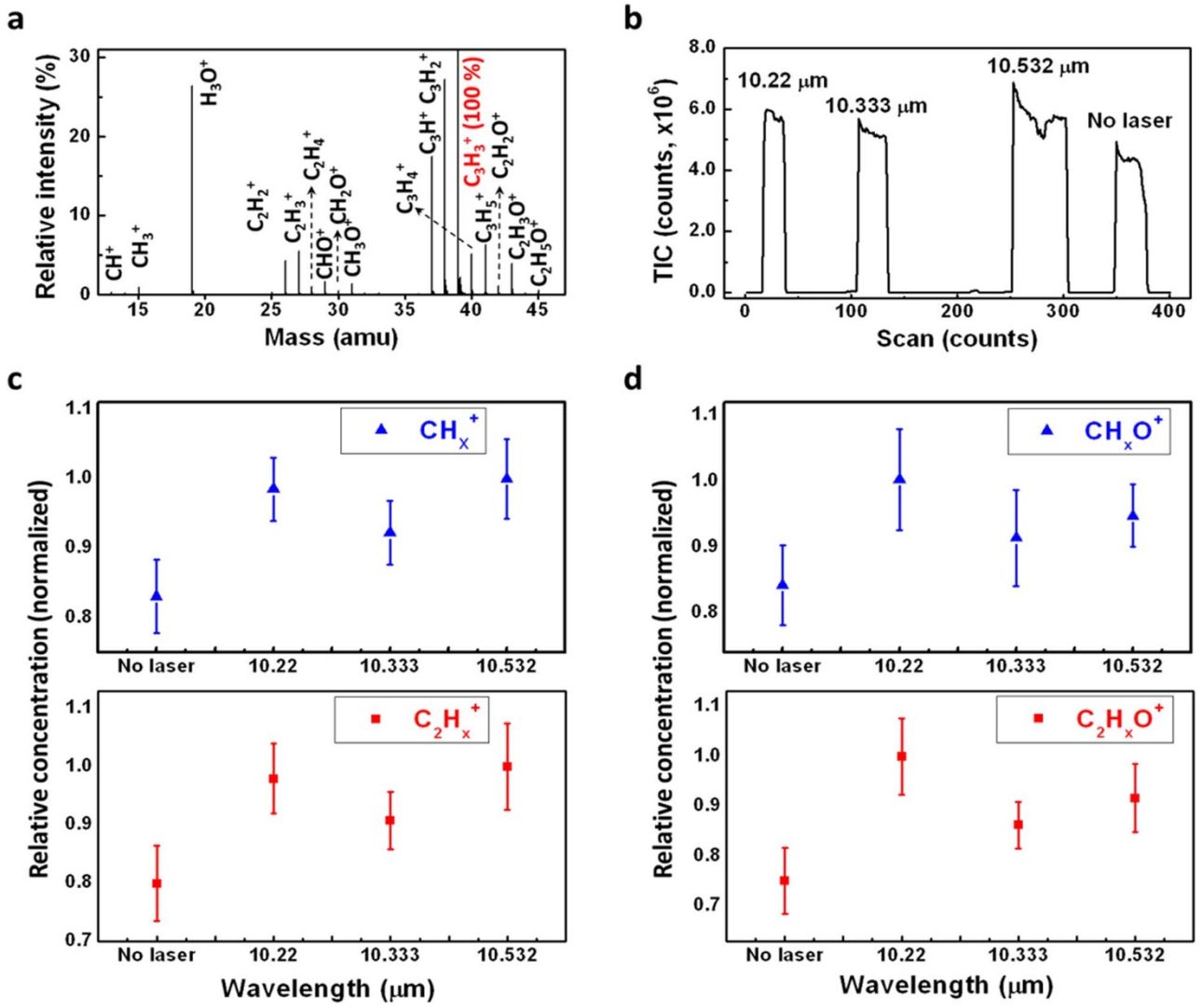


**Figure 4 | Mass spectrometry of the $C_2H_4/C_2H_2/O_2$ flame.** (a), Mass spectrum of the flame irradiated with $CO_2$ laser at 10.22 μm. (b), Total ion current of the flame under different excitation conditions. (c), (d), Relative concentrations of $CH_x$ (x = 0 ~ 3), $C_2H_x$ (x = 0 ~ 5) ions (c), and $CH_xO$ (x = 1 ~ 3), $C_2H_xO$ (x = 2 ~ 5) ions (d).

the ⟨100⟩ direction. This favorable adsorption of hydrocarbon species on C{111}-1 × 1 surface over the C{100}-2 × 1 reconstruction surface is very similar to H- and OH- adsorptions on the relevant diamond surfaces[36–38]. Keep in mind that faster growth of one axial direction of crystals will result in larger areas of adjacent facets[14,32]. In this case, the growth rate in the ⟨111⟩ direction is higher than that in the ⟨100⟩ direction, resulting in larger area of the adjacent C{100} facets, which explains the predominant appearance of the diamond {100} surfaces.

To summarize, we have demonstrated a laser-assisted combustion process to synthesize {100}-oriented diamond films and single crystals through resonant vibrational excitation of precursor molecules. The $CO_2$ laser beam at 10.22 μm excites the ethylene molecules to a higher vibrational state with higher rotational energy in the combustion flame, which increases the relative concentrations of the $CH_xO$ and $C_2H_xO$ species. Theoretical simulations of the reaction pathway indicate that these species react more easily with diamond {111} surfaces than with {100} surfaces, leading to a fast growth in the ⟨111⟩ direction and resulting in {100}-oriented diamond. This finding opens up a new avenue for controlled chemical vapor deposition of crystals through resonant vibrational excitation of precursor molecules.

Table 1 | Calculated chemisorption energies (eV) on Diamond {100} and {111} surface with PBE/DNP method

| Molecule | Chemisorption energy (eV) | |
|---|---|---|
| | On C{100} | On C{111} |
| CHO | −2.58 | −3.28 |
| $CH_2O$ | −2.64 | −3.27 |
| $CH_3O$ | −2.83 | −3.53 |
| $C_2H$ | −4.43 | −5.53 |
| $C_2H_2$ | −3.75 | −4.60 |
| $C_2H_3$ | −3.84 | −5.78 |
| $C_2H_2O$ | −3.13 | −3.99 |
| $C_2H_3O$ | −4.69 | −6.49 |
| $C_2H_5O$ | −6.09 | −3.53 |
| $C_3H$ | −4.04 | −4.34 |
| $C_3H_2$ | −4.06 | −4.93 |
| $C_3H_3$ | −2.35 | −2.76 |
| $C_3H_4$ | −3.62 | −4.34 |
| $C_3H_5$ | −5.18 | −6.35 |

## Methods

**Diamond synthesis.** A combustion torch with a 1.5 mm orifice tip was used to produce the flame. The precursor gases consisted of a mixture of $C_2H_4$ (99.999%), $C_2H_2$ (99.6%), and $O_2$ (99.996%), which were mixed in the torch through three gas flow meters (B7920V, Spec-Air Gases & Technologies). The gas flow rates of $C_2H_4$, $C_2H_2$, and $O_2$ were 0.62, 0.62, and 1.20 standard liters per minute (slpm), respectively. The $CO_2$ laser beam used to irradiate the flame was parallel with the substrate surfaces. A ZnSe convex lens with a focal length of 256 mm was used to focus the laser beam from its original diameter of ~13 mm to ~2 mm which is similar to the diameter of the flame (Figure 1a). The laser power density at the flame was around $3 \times 10^4$ W/cm$^2$. A tungsten carbide (WC) substrate (BS-6S, Basic Carbide Corp., containing 6% cobalt) with a dimension of $12.7 \times 12.7 \times 1.6$ mm$^3$ was placed on a water-cooled brass box mounted on an X-Y-Z stage. The surface roughness of the WC substrate was 400 nm. The substrate was cleaned in a supersonic bath of acetone for 15 min before diamond deposition. The distance between the substrate surface and the inner cone of the flames was about 0.5 mm in all experiments. The temperature of the substrate during deposition was maintained at 770 ~ 780°C and monitored by a noncontact pyrometer (OS3752, Omega Engineering, Inc.). Raman spectroscopy was performed for the diamond samples using a Renishaw Raman spectrometer (inVia 9F5803) with an argon ion laser as the excitation source (514.5 nm, 100 mW).

**Mass spectrometry.** Positive ions in the $C_2H_4/C_2H_2/O_2$ flame were detected using a time-of-flight mass spectrometer (MS, AccuTOF$^{TM}$, JEOL USA, Inc.), as shown in Figure S2 in the Supplementary Information. A stainless steel orifice with an inner diameter of 400 μm on the mass spectrometer collects ions in open air. The combustion torch was fixed on a motorized X-Y-Z stage and the relative position of the flame to the orifice was precisely adjusted so that the tip of the flame inner cone was right at front of the orifice under all excitation conditions. The flame-to-orifice distance for the MS detection was the same as the flame-to-substrate distance for diamond deposition. In this way, the detected species are believed to be the same as what exist in the diamond growth. The MS data were analyzed using the TSSPro software (Shrader Analytical and Consulting Laboratories, Inc. Version 3.0) and the MS Tools software (JEOL USA, Inc.).

**Computation of chemisorption.** The chemisorption energies were calculated using the density functional theory (DFT). We constructed a slab containing 8 atomic layers of $4 \times 4$ diamond {111}-$1 \times 1$ surface (where the lower 4 atomic layers are fixed and the top 4 atomic layers are fully relaxed) and another slab containing 9 atomic layers of $4 \times 4$ {100}-$2 \times 1$ reconstruction surface (where the lower 4 atomic layers are fixed and top 5 atomic layers are fully relaxed). Each layer has 16 carbon atoms and the lower 4 layers are not terminated. Note that the slab models constructed here are very close to the models reported in the literatures[36–38]. The vacuum slab in the supercell was set as 20 Å. The DFT calculations are based on the Perdew-Burke-Ernzerhof (PBE)[39] functional at double numerical polarized (DNP) basis sets[40,41]. The DNP basis sets are considered as superior as the Gaussian 6-311+G(3 df,2 pd) basis sets[42], confirming reliability of our DFT calculations. The energy convergence was set as $10^{-6}$ Hartree, and the energy convergence for the geometrical optimization was set as $1 \times 10^{-5}$ Hartree. The chemisorption energies were evaluated as: E(chemisorption) = $E(C_nH_mO_k - \text{surface}) - E(C_nH_mO_k) - E(\text{surface})$. All calculations were carried out using the DMol$^3$ 6.0 program software[40,41].


1. Crim, F. F. Making Energy Count. *Science* **317**, 1707–1708 (2007).
2. Potter, E. D., Herek, J. L., Pedersen, S., Liu, Q. & Zewail, A. H. Femtosecond laser control of a chemical reaction. *Nature* **355**, 66–68 (1992).
3. Bechtel, H. A., Kim, Z. H., Camden, J. P. & Zare, R. N. Bond and mode selectivity in the reaction of atomic chlorine with vibrationally excited $CH_2D_2$. *J. Chem. Phys.* **120**, 791–799 (2004).
4. Zhang, W. Q., Kawamata, H. & Liu, K. P. CH Stretching Excitation in the Early Barrier F + $CHD_3$ Reaction Inhibits CH Bond Cleavage. *Science* **325**, 303–306 (2009).
5. Killelea, D. R., Campbell, V. L., Shuman, N. S. & Utz, A. L. Bond-Selective Control of a Heterogeneously Catalyzed Reaction. *Science* **319**, 790–793 (2008).
6. Zare, R. N. Laser Control of Chemical Reactions. *Science* **279**, 1875–1879 (1998).
7. Butkus, M. *et al.* High-power quantum-dot-based semiconductor disk laser. *Opt. Lett.* **34**, 1672–1674 (2009).
8. Dore, P. *et al.* Infrared Properties of Chemical-Vapor Deposition Polycrystalline Diamond Windows. *Appl. Opt.* **37**, 5731–5736 (1998).
9. Dankerl, M. *et al.* Diamond Transistor Array for Extracellular Recording From Electrogenic Cells. *Adv. Funct. Mater.* **19**, 2915–2923 (2009).
10. Liao, M., Hishita, S., Watanabe, E., Koizumi, S. & Koide, Y. Suspended Single-Crystal Diamond Nanowires for High-Performance Nanoelectromechanical Switches. *Adv. Mater.* **22**, 5393–5397 (2010).
11. Henderson, M. R. *et al.* Diamond in Tellurite Glass: a New Medium for Quantum Information. *Adv. Mater.* **23**, 2806–2810 (2011).
12. Prawer, S. & Greentree, A. D. Diamond for Quantum Computing. *Science* **320**, 1601–1602 (2008).
13. Balasubramanian, G. *et al.* Ultralong spin coherence time in isotopically engineered diamond. *J. Nature Mater.* **8**, 383–387 (2009).
14. Liu, T., Raabe, D., Mao, W. & Zaefferer, S. Microtexture and Grain Boundaries in Freestanding CVD Diamond Films: Growth and Twinning Mechanisms. *Adv. Funct. Mater.* **19**, 3880–3891 (2009).
15. Butler, J. E. & Oleynik, I. A mechanism for crystal twinning in the growth of diamond by chemical vapour deposition. *Phil. Trans. R. Soc. A* **366**, 295–311 (2008).
16. Avigal, Y., Glozman, O., Etsion, I., Halperin, G. & Hoffman, A. [100]-Textured diamond films for tribological applications. *Diam. Relat. Mater.* **6**, 381–385 (1997).
17. Su, Q. F., Xia, Y. B., Wang, L. J., Liu, J. M. & Shi, W. M. Influence of texture on optical and electrical properties of diamond films. *Vacuum* **81**, 644–648 (2007).
18. Schade, A., Rosiwal, S. M. & Singer, R. F. Influence of surface topography of HF-CVD diamond films on self-mated planar sliding contacts in dry environments. *Diam. Relat. Mater.* **15**, 1682–1688 (2006).
19. Fabisiak, K., Banaszak, A., Kaczmarski, M. & Kozanecki, M. Paramagnetic defects in diamond films synthesized by the hot filament chemical vapour deposition. *Cryst. Res. Technol.* **41**, 535–540 (2006).
20. Stoner, B. R., Sahaida, S. R., Bade, J. P., Southworth, P. & Ellis, P. J. Highly oriented, textured diamond films on silicon via bias-enhanced nucleation and textured growth. *J. Mater. Res.* **8**, 1334–1340 (1993).
21. Fox, B. A. *et al.* Epitaxial nucleation, growth and characterization of highly oriented, (100)-textured diamond films on silicon. *Diam. Relat. Mater.* **3**, 382–387 (1994).
22. Locher, R., Wild, C., Herres, N., Behr, D. & Koidl, P. Nitrogen stabilized <100> texture in chemical vapor deposited diamond films. *Appl. Phys. Lett.* **65**, 34–36 (1994).
23. Edmonds, A. M. *et al.* Production of oriented nitrogen-vacancy color centers in synthetic diamond. *Phys. Rev. B* **86**, 035201 (2012).
24. Pham, L. M. *et al.* Enhanced metrology using preferential orientation of nitrogen-vacancy centers in diamond. *Phys. Rev. B* **86**, 121202(R) (2012).
25. Tang, C. J., Fernandes, A. J. S., Costa, F. & Pinto, J. L. Effect of microwave power and nitrogen addition on the formation of {100} faceted diamond from microcrystalline to nanocrystalline. *Vacuum* **85**, 1130–1134 (2011).
26. Ayres, V. M. *et al.* The effect of nitrogen on competitive growth mechanisms of diamond thin films. *Diam. Relat. Mater.* **9**, 236–240 (2000).
27. Ling, H. *et al.* Enhanced chemical vapor deposition of diamond by wavelength-matched vibrational excitations of ethylene molecules using tunable $CO_2$ laser irradiation. *J. Appl. Phys.* **105**, 064901 (2009).
28. Xie, Z. Q. *et al.* Fast Growth of Diamond Crystals in Open Air by Combustion Synthesis with Resonant Laser Energy Coupling. *Cryst. Growth Des.* **10**, 1762–1766 (2010).
29. Gallaway, W. S. & Barker, E. F. The Infra-Red Absorption Spectra of Ethylene and Tetra-Deutero-Ethylene under High Resolution. *J. Chem. Phys.* **10**, 88–97 (1942).
30. Xing, X. *et al.* Rovibrationally selected and resolved state-to-state photoionization of ethylene using the infrared-vacuum ultraviolet pulsed field ionization-photoelectron method. *J. Chem. Phys.* **125**, 133304 (2006).
31. Steeds, J. W., Gilmore, A., Wilson, J. A. & Butler, J. E. On the nature of extended defects in CVD diamond and the origin of compressive stresses. *Diam. Relat. Mater.* **7**, 1437–1450 (1998).
32. Asmussen, J. & Reinhard, D. K. *Diamond Films Handbook* Ch. 4 (Marcel Dekker, New York, 2002).
33. Bäuerle, D. *Laser Processing and Chemistry* Ch. 2 (Springer-Verlag, Berlin Heidelberg, 2000).
34. Hansgen, D. A., Vlachos, D. G. & Chen, J. G. Using first principles to predict bimetallic catalysts for the ammonia decomposition reaction. *Nature Chem.* **2**, 484–489 (2010).
35. Vogel, D. *et al.* Local Catalytic Ignition during CO Oxidation on Low-Index Pt and Pd Surfaces: A Combined PEEM, MS, and DFT Study. *Angew. Chem. Int. Ed.* **57**, 10041–10044 (2012).
36. Petrini, D. & Larsson, K. A Theoretical Study of the Energetic Stability and Geometry of Hydrogen- and Oxygen-Terminated Diamond (100) Surfaces. *J. Phys. Chem. C* **111**, 795–801 (2007).
37. Petrini, D. & Larsson, K. Electron-Transfer Doping on a (001) Surface of Diamond: Quantum Mechanical Study. *J. Phys. Chem. B* **109**, 22426–22431 (2005).
38. Petrini, D. & Larsson, K. Theoretical Study of the Thermodynamic and Kinetic Aspects of Terminated (111) Diamond Surfaces. *J. Phys. Chem. C* **112**, 3018–3026 (2008).
39. Perdew, J. P., Burke, K. & Ernzerhof, M. Generalized gradient approximation made simple. *Phys. Rev. Lett.* **77**, 3865–3868 (1996).
40. Delley, B. An all-electron numerical method for solving the local density functional for polyatomic molecules. *J. Chem. Phys.* **92**, 508–517 (1990).
41. Delley, B. From molecules to solids with the DMol3 approach. *J. Chem. Phys.* **113**, 7756–7764 (2000).
42. Inada, Y. & Orita, H. Efficiency of numerical basis sets for predicting the binding energies of hydrogen bonded complexes: Evidence of small basis set superposition error compared to Gaussian basis sets. *J. Comput. Chem.* **29**, 225–232 (2008).


## Acknowledgments

The authors would like to thank Dr. D.R. Alexander from the Department of Electrical Engineering at the University of Nebraska-Lincoln for providing convenient access to his SEM. This work was financially supported by the U. S. Office of Naval Research (ONR, grant N00014-09-1-0943) and National Science Foundation (CMMI 0852729, 1068510,

and 1129613). We are grateful to Dr. I. Perez at ONR for his advice and support which enabled the progress of the programs during the past years.

## Author contributions

The first four authors contribute equally to this research. Z.X., J.P. and T.G. carried out the deposition and characterization of diamond films. J.B. and Y.G. carried out the theoretical simulations. Z.X. performed the MS analysis of the reaction. Z.X. and Y.Z. wrote the manuscript. Y.L., X.Z. and L.J. planned and supervised the study. All authors discussed the results and commented on the manuscript.

## Additional information

**Supplementary information** accompanies this paper at http://www.nature.com/scientificreports

**Competing financial interests:** The authors declare no competing financial interests.

**How to cite this article:** Xie, Z.Q. *et al*. Control of crystallographic orientation in diamond synthesis through laser resonant vibrational excitation of precursor molecules. *Sci. Rep.* **4**, 4581; DOI:10.1038/srep04581 (2014).